The Inhibitory Action of Phospholamban Involves Stabilization of α-Helices within the Ca-ATPase†

Suren A. Tatulian,*,‡,§ Baowei Chen,‡,▽ Jinhui Li,‡,▽ Sewite Negash,‡,|| C. Russell Middaugh,⊥ Diana J. Bigelow,‡,▽ and Thomas C. Squier‡,▽

Biochemistry and Biophysics Section, Department of Molecular Biosciences, and Department of Pharmaceutical Chemistry, University of Kansas, Lawrence, Kansas 66045-2106

Received June 4, 2001; Revised Manuscript Received September 28, 2001

ABSTRACT: We have used attenuated total reflection Fourier transform infrared (ATR-FTIR) and circular dichroism (CD) spectroscopies to identify secondary and dynamic structural changes within the Ca-ATPase that result from the functional inhibition of transport activity by phospholamban (PLB). Isotopically labeled [^{13}C]PLB was expressed and purified from *Escherichia coli* and was functionally reconstituted with unlabeled Ca-ATPase, permitting the resolution of the amide I and II absorbance bands of the Ca-ATPase from those of [^{13}C]PLB. Upon co-reconstitution of the Ca-ATPase with PLB, spectral shifts are observed in both the CD spectra and the amide I and II bands associated with the Ca-ATPase, which are indicative of increased α-helical stability. Corresponding changes in the kinetics of H/D exchange occur upon association with PLB, indicating that 100 ± 20 residues in the Ca-ATPase that normally undergo rapid amide H/D exchange become exchange resistant. There are no corresponding large changes in the secondary structure of PLB. The affinity of the structural interaction between PLB and the Ca-ATPase is virtually identical to that associated with functional inhibition (K_d = 140 ± 30 μM), confirming that the inhibitory regulation of the Ca-ATPase by PLB involves the stabilization of α-helices within the Ca-ATPase.

The β-adrenergic cascade in the heart acts to enhance the rate of calcium resequestration into the sarcoplasmic reticulum (SR)[1] lumen through the direct phosphorylation of phospholamban (PLB) at either Ser^{16} or Thr^{17} by cAMP-dependent protein kinase (PKA) or calmodulin-dependent protein kinase, respectively (*1*−*5*). Phosphorylation of PLB results in a shift in the calcium dependence of the catalytic activity of the Ca-ATPase toward lower sub-micromolar free calcium concentrations with little or no alteration in the maximal velocity of the Ca-ATPase (*6*−*8*). The similarity between the calcium dependence of Ca-ATPase transport activity found in the activated cardiac SR (after phosphorylation of PLB) and that of the Ca-ATPase found in the skeletal muscle SR (in which PLB is not expressed) suggests that dephosphorylated PLB acts as an inhibitor of the Ca-ATPase (*1*). Direct assessments of calcium binding and detailed kinetic measurements indicate that PLB does not alter calcium affinity, but rather alters the activation barrier associated with the slow isomerization step of calcium activation (*9*, *10*). Structural coupling between PLB and the Ca-ATPase in cardiac SR membranes involves direct contact interactions in both the cytoplasmic and transmembrane domains (*11*). The cardiac isoform of the Ca-ATPase, SERCA2a, contains a sequence near the nucleotide binding cleft, i.e., Lys-Asp-Asp-Lys-Pro-Val-Lys^{402}, that is required for the functional interaction between PLB and the Ca-ATPase (*7*, *12*, *13*), suggesting that these residues may comprise a critical binding region. The homologous SERCA1 isoform of rabbit skeletal muscle has a similar sequence, Lys-Asn-Asp-Lys-Pro-Ile-Arg^{402}, and when co-reconstituted with PLB is similarly regulated by changes in the phosphorylation of PLB. Specific binding sites within transmembrane helix M6 of the SERCA1 isoform of the Ca-ATPase have been identified that interact with PLB transmembrane sequences, and coexpression of the transmembrane sequence alone of PLB with the Ca-ATPase has been shown to inhibit transport activity at sub-micromolar calcium concentrations (*11*, *14*).

Spectroscopic studies, primarily involving the covalent attachment of either spin-label or optical probes to either PLB or the Ca-ATPase, have revealed changes in the tertiary or quaternary structure of these proteins that are associated with their functional interaction (*10*, *15*−*18*). Possible

† Supported by National Institutes of Health Grant HL64031 and the American Heart Association.

* To whom correspondence should be addressed. Telephone: (407) 207-4996. Fax: (407) 384-2816. E-mail: statulia@mail.ucf.edu.

‡ Department of Molecular Biosciences.

§ Present address: Center for Discovery of Drugs and Diagnostics, University of Central Florida, Orlando, FL 32826.

|| Present address: LMDB, National Eye Institute, Bethesda, MD 20892.

⊥ Department of Pharmaceutical Chemistry.

▽ Present address: Pacific Northwest National Laboratory, Richland, WA 99352.

[1] Abbreviations: ATR-FTIR, attenuated total reflection Fourier transform infrared; BAPTA, 1,2-bis(2-aminophenoxy)ethane-*N*,*N*,*N*′,*N*′-tetraacetic acid; β-OG, *N*-octyl β-D-glucopyranoside; cAMP, adenosine 3,5-cyclic monophosphate; Ca-ATPase, Ca^{2+}- and Mg^{2+}-dependent ATPase; $C_{12}E_9$, polyoxyethylene 9-lauryl ether; CCCP, carbonyl cyanide 3-chlorophenylhydrazone; CD, circular dichroism; DEAE, diethylaminoethyl; EGTA, ethylene glycol bis(β-aminoethyl ether)-*N*,*N*,*N*′,*N*′-tetraacetic acid; GST, glutathione *S*-transferase; MOPS, 3-(*N*-morpholino)propanesulfonic acid; PAGE, polyacrylamide gel electrophoresis; PKA, cAMP-dependent protein kinase; PLB, phospholamban; SERCA, sarco(endo)plasmic reticulum Ca-ATPase; SDS, sodium dodecyl sulfate; SR, sarcoplasmic reticulum.

10.1021/bi011148d CCC: $22.00
Published on Web 12/27/2001

conformational alterations, however, involving secondary structural elements in both the Ca-ATPase and PLB upon their functional interaction have not previously been studied. Therefore, in this study, we have used CD and ATR-FTIR spectroscopies to detect possible secondary structural changes of the Ca-ATPase and [^{13}C]PLB following their functional co-reconstitution. CD measures the average secondary structure of the complex between the Ca-ATPase and PLB, but does not provide information on individual structural changes in either protein resulting from their interaction. On the other hand, FTIR spectroscopy measures various vibrational absorbance bands that are sensitive either to the protein backbone conformation (e.g., the amide I band between 1700 and 1600 cm^{-1}) or the amide hydrogen-deuterium (H/D) exchange and solvent accessibility (e.g., the amide II band between 1580 and 1520 cm^{-1}). Thus, FTIR spectroscopy is complementary to CD and permits measurement of the secondary and dynamic structures of proteins. Moreover, by isotopically labeling one of the proteins (e.g., by ^{13}C) FTIR can be used to measure the individual structures of two interacting proteins. The spectral shift of both amide I and amide II bands toward lower frequencies (by ~50 and 20 cm^{-1}, respectively) resulting from ^{13}C-labeling makes it possible to obtain structural information on both proteins in the same sample by analyzing the separated bands generated by the labeled and unlabeled proteins. In the case of membrane proteins, ATR-FTIR spectroscopy permits selective detection of proteins associated with supported membranes (*19*).

Using ATR-FTIR, we have resolved structural changes within the Ca-ATPase resulting from interaction with ^{13}C-labeled PLB that involve the stabilization of α-helical secondary structural elements. Although this approach has previously been applied to study interactions between water-soluble proteins and peptides by direct transmission FTIR spectroscopy (*20*, *21*), no previous measurements have been reported involving the use of isotope-edited infrared spectroscopy in investigating structural interactions between integral membrane proteins. These PLB-induced changes in the structure of the Ca-ATPase are suggested to contribute to the inhibition of its transport activity by increasing the activation barrier associated with calcium activation that is necessary to promote nucleotide utilization.

MATERIALS AND METHODS

Materials. $CaCl_2$ standard solutions were purchased from VWR (St. Louis, MO). MOPS, KCl, and ultracentrifugation grade sucrose were purchased from Fisher (Fair Lawn, NJ). Reactive red 120 and the detergent *N*-octyl β-D-glucopyranoside (β-OG) were obtained from ICN (Aurora, OH). [U-$^{13}C_6$]-D-Glucose was obtained from Cambridge Isotope Laboratories (Andover, MA). Sepharose CL-4B, the detergent $C_{12}E_9$ (polyoxyethylene 9-lauryl ether), ADP, PKA, cAMP, ATP, $MgCl_2$, the calcium ionophore A23187, the potassium ionophore valinomycin, and EGTA were purchased from Sigma (St. Louis, MO). The protonophore CCCP (carbonyl cyanide 3-chlorophenylhydrazone) was purchased from Fluka (Buchs, Switzerland). Dansyl chloride [1-(dimethylamino)naphthalene-5-sulfonyl chloride] and the calcium sensitive dye BAPTA [1,2-bis(2-aminophenoxy)-ethane-*N*,*N*,*N*′,*N*′-tetraacetic acid] were purchased from Molecular Probes (Eugene, OR). SR vesicles were isolated from either rabbit skeletal fast twitch muscle or porcine hearts as described previously (*10*, *22*). Lipids were extracted from skeletal SR vesicles with organic solvents as previously described (*23*, *24*). Ca-ATPase from skeletal SR was affinity purified essentially as previously described (*25*, *26*). Native and reconstituted vesicles containing the Ca-ATPase were stored at −70 °C.

Expression and Purification of PLB. PLB was cloned into a pGEX-2T plasmid expression vector, expressed in JM109 *Escherichia coli* cells, and purified by preparative SDS−PAGE, essentially as previously described (*27*). In this construction, the N-terminus of PLB was modified to introduce a thrombin cleavage site. For this reason, the expressed PLB contains a Gly-Ser sequence in place of Met at the N-terminus. For preparation of uniformly ^{13}C-labeled PLB, the cells were grown in a minimal M9 medium containing 2 g/L [U-$^{13}C_6$]-D-glucose as the sole carbon source. The cells were harvested by centrifugation when A_{600} was at least 1.2 and resuspended in urea buffer [20 mM Tris (pH 8.4), 0.5 M NaCl, and 4 M urea], and the cells were disrupted by a procedure involving five freeze−thaw cycles using liquid nitrogen and sonication for 1 min. A membrane fraction was obtained following centrifugation at 37000g_{max} for 15 min using a SS-34 rotor, and the resulting pellet was resuspended in the cell lysis buffer and again subjected to the cell disruption and centrifugation procedure. The resulting pellet was resuspended in 30 mL of SDS-denaturing buffer [100 mM Tris (pH 6.8), 4% SDS, 5% 2-mercaptoethanol, 0.45 M sucrose, and 0.001% bromophenol blue] and sonicated as described above. Following centrifugation for 15 min at 37000g_{max}, the GST−PLB fusion protein was separated from other proteins in the supernatant by preparative SDS−PAGE using 10 mM Tris (pH 8.3), 0.2 M glycine, and 0.1% SDS as the running buffer. Fractions containing the GST−PLB protein were identified by analytical SDS−PAGE. The yield was approximately 13 mg of GST−PLB protein from 1 L of *E. coli* culture. The GST−PLB fusion protein was cleaved to GST and PLB using freshly prepared human thrombin (30 units of thrombin/mg of protein) for 48 h at room temperature, followed by lyophilization. The lyophilized sample was solubilized in 5 mL of 1 mM $MgCl_2$, 50 mM $CaCl_2$, and 20% glycerol, boiled for 15 min, and separated by preparative electrophoresis. Fractions containing PLB were collected and lyophilized, yielding approximately 1.8 mg of [^{13}C]PLB. The anionic detergent (SDS) in the lyophilized sample was replaced with nonionic $C_{12}E_9$ by first solubilizing the sample in 20 mM MOPS (pH 7.0) and 1% $C_{12}E_9$ prior to applying the sample to a DEAE-cellulose column ($V_t \approx 1$ mL) pre-equilibrated with the same buffer. Following extensive washing, PLB was eluted from the column by adding 0.2 M NaCl to the $C_{12}E_9$ solubilization buffer as a mixture of monomeric, trimeric, tetrameric, and pentameric forms as identified by SDS−PAGE (*27*). Subsequent reconstitution of the detergent-purified PLB into lipids restores the preference for pentameric and monomeric species characteristic of cardiac SR membranes, suggesting that detergent micelles may prevent free exchange of PLB between different oligomeric species.

Co-Reconstitution of the Ca-ATPase with PLB. The purified Ca-ATPase was reconstituted in the presence of variable amounts of PLB into lipids extracted from SR membranes, with minor modifications to established proto-

cols (*28*, *29*). Prior to reconstitution, 1.1 mg of extracted SR lipids was dried under nitrogen gas and kept in a vacuum desiccator overnight. The dried SR lipids were suspended in approximately 0.5 mL of reconstitution buffer [20 mM MOPS (pH 7.0), 0.1 M KCl, 0.1 mM $CaCl_2$, and 0.3 M sucrose] and solubilized by adding 1.7 mM octyl glucoside. Separately, 200 μg (1.8 nmol) of purified Ca-ATPase was mixed with 9, 18, and 27 nmol of PLB solubilized in 4 mg/mL $C_{12}E_9$ (or an equivalent volume of 4 mg/mL $C_{12}E_9$ when the Ca-ATPase was reconstituted without PLB) in a final volume of 100 μL. This mixture was then combined with the solubilized SR lipids, resulting in a final volume of 0.6 mL containing 1.4 mM octyl glucoside and 0.7 mg/mL $C_{12}E_9$. To remove the detergent, 100 mg of SM-2 Bio-Beads (Bio-Rad, Richmond, CA) was added, and the solution was incubated with gentle stirring for 1 h. Two more 100 mg aliquots of Bio-Beads were added at 1 h intervals. The resulting reconstituted vesicles were removed from the Bio-Beads and concentrated by centrifugation at 300000g_{max} for 15 min. The final lipid-to-protein ratio was 750 phospholipids per Ca-ATPase. The in situ molar ratio between the co-reconstituted Ca-ATPase and PLB was estimated using the areas of the corresponding amide I bands in the ATR-FTIR spectra, assuming similar extinction coefficients for both proteins. In separate experiments, the molar ratios of PLB relative to the Ca-ATPase were confirmed using quantitative immunoblotting to measure the concentrations of the Ca-ATPase and PLB. The measurements involved the use of purified Ca-ATPase and PLB as protein standards using primary monoclonal mouse antibodies raised against the Ca-ATPase from fast twitch skeletal muscle (IgG1 clone 11H11 from Affinity Bioreagents, Golden, CO) and recombinant PLB (clone 8A3) prepared in our laboratory from hybridoma cells derived from ascites fluid using standard protocols. Following absorption of either native or reconstituted vesicles to PVDF membranes, the immunoreactivity of various protein loads was quantified following color development using goat anti-mouse IgG−alkaline phosphatase secondary antibody (Affinity Bioreagents). To correct for differences in binding affinities of antibodies directed against either the Ca-ATPase or PLB, linear standard curves were obtained in which the immunoreactivity of the antibody was measured against purified Ca-ATPase or PLB, permitting a determination of the amount of either the Ca-ATPase or PLB.

Using ATR-FTIR, we found that addition of a 5-, 10-, and 15-fold molar excess of PLB relative to the Ca-ATPase results in in situ molar ratios of approximately 1:1, 4:1, and 11:1 in the supported bilayers, respectively. Furthermore, the amide I signal of [^{13}C]PLB when co-reconstituted with the Ca-ATPase was stronger than when reconstituted alone at the same input concentrations, implying that the Ca-ATPase is preferentially incorporated into the phospholipid membranes, and facilitates reconstitution of PLB. Similar results were obtained using quantitative immunoblotting to measure the relative concentrations of the Ca-ATPase and PLB, confirming the reliability of both methods.

Preparation of Supported Lipid Bilayers. Supported lipid bilayers were prepared essentially as described previously (*30*). Prior to the addition of proteoliposomes, a phospholipid monolayer was deposited on a 1 mm × 20 mm × 50 mm germanium internal reflection plate (Spectral Systems, Irvington, NY) using a Langmuir-Blodgett monolayer trough (model 611, Nima, Coventry, England). Following assembly of the plate with the monolayer in a perfusable liquid ATR cell (Buck Scientific, East Norwalk, CT), vesicles with (co-)reconstituted protein(s) were injected into the ATR cell and incubated for approximately 1.5 h to allow the vesicles to spread onto the lipid monolayer and yield supported phospholipid bilayers that incorporate the reconstituted protein(s).

Enzymatic and Protein Assays. ATP hydrolysis activity of the Ca-ATPase was determined by assessing the release of inorganic phosphate (*31*), using 100 μg of protein/mL in a solution containing 50 mM MOPS (pH 7.0), 0.1 M KCl, 5 mM $MgCl_2$, 1 mM EGTA, 2 μM A23187, 1 μM CCCP, 2 μM valinomycin, 0.3 M sucrose, and sufficient calcium to yield the desired concentration of free calcium. In experiments where the effect of the phosphorylation of PLB on Ca-ATPase activity was measured, 10 μg of PKA/mL and 1 μM cAMP were also included in the assay buffer. The solution was incubated at 25 °C for 10 min prior to the addition of 5 mM ATP to start the reaction. The extent of PLB phosphorylation induced by PKA involved incubation of proteoliposomes for 10 min in the presence of [γ-^{32}P]ATP (4500 cpm/nmol) and 0.5 μM free calcium. The reaction was stopped by filtration on a glass filter, followed by washing with nonradioactive reaction buffer. The amount of radioactivity associated with each filter was measured by scintillation counting. The amount of nonspecific radioactivity measured in the absence of PKA was subtracted from the total amount of radioactivity. Protein concentrations of PLB stocks were determined by amino acid analysis. All other protein concentrations were determined by the amido black method (*32*).

Covalent Attachment of Spectroscopic Probes to PLB. Recombinant PLB (200 μg) in 4 mg/mL $C_{12}E_9$ and 20 mM MOPS (pH 8.0) was incubated with a 20-fold molar excess of dansyl chloride for 5 h in the dark at room temperature. The reaction was stopped by addition of a 10-fold excess of lysine, and prior to exhaustive dialysis, the solution was incubated for an additional 45 min to bind the unreacted probe. Following exhaustive dialysis against 2 mg/mL $C_{12}E_9$ and 20 mM MOPS (pH 7.0), the stoichiometry of labeling was determined from the molar extinction coefficient [ϵ_{344} = 4600 M^{-1} cm^{-1} (*33*)].

Determination of Calcium Binding Affinities. To analyze the relative affinities and cooperative interactions between high-affinity calcium binding sites on the Ca-ATPase, the calcium-dependent activation of the Ca-ATPase was fit to the following equation:

$$\text{ATPase activity} = \frac{K_1[Ca^{2+}]_{free} + 2K_2[Ca^{2+}]_{free}^{\ 2}}{2(1 + K_1[Ca^{2+}]_{free} + K_2[Ca^{2+}]_{free}^{\ 2})} \quad (1)$$

ATPase activity represents the measured calcium-dependent ATPase activity and is assumed to result from the fraction of Ca-ATPase polypeptide chains in which both high-affinity calcium sites are occupied by calcium. K_1 corresponds to the sum of the intrinsic equilibrium constants associated with calcium binding to the two high-affinity binding sites on the Ca-ATPase (k_1 and k_2). K_2 represents the product of intrinsic

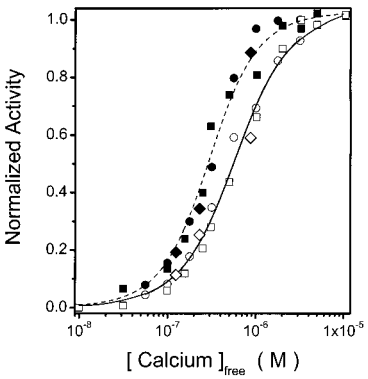

FIGURE 1: Rates of ATP hydrolysis by the Ca-ATPase in native cardiac SR membranes (□ and ■) or of the Ca-ATPase co-reconstituted with either [^{12}C]PLB (○ and ●) or [^{13}C]PLB (◇ and ◆) before (white symbols) and following (black symbols) PLB phosphorylation by PKA. Data for native cardiac SR are taken from ref *10*. Experimental curves were obtained using eq 1 before (−) and following (- - -) PLB phosphorylation. The macroscopic equilibrium constants K_1 and K_2 before PLB phosphorylation are $(1.5 \pm 0.4) \times 10^6$ M^{-1} and $(3.0 \pm 0.4) \times 10^{12}$ M^{-2} and following PLB phosphorylation are $(1.9 \pm 0.7) \times 10^6$ M^{-1} and $(1.1 \pm 0.1) \times 10^{13}$ M^{-2}, respectively. Standard deviations of individual measurements are no more than 8% of the indicated values. Maximal calcium-dependent ATPase activities determined from a global fit to data sets obtained before and after enzyme activation resulting from the addition of PKA were 4.0 ± 0.1 and 1.0 ± 0.1 μmol of P_i mg^{-1} min^{-1} for the Ca-ATPase co-reconstituted with PLB and cardiac SR membranes, respectively.

equilibrium constants k_1, k_2, and k_c, and explicitly takes into consideration cooperative interactions (k_c) between the high-affinity calcium binding sites (*34*).

Determination of PLB Binding Affinity. The concentration of unbound PLB was obtained from the following relationship:

$$[\text{PLB}]_{\text{free}} = [\text{PLB}]_{\text{total}} - \frac{\Delta K_{\text{Ca}}}{\Delta K_{\text{Ca}}(\text{max})}[\text{Ca-ATPase}]_{\text{total}} \quad (2)$$

where $\Delta K_{\text{Ca}}/\Delta K_{\text{Ca}}(\text{max})$ corresponds to the fraction of Ca-ATPase associated with PLB and represents the observed shift in the calcium concentration associated with half-maximal activation of the Ca-ATPase relative to the maximal shift observed in the presence of excess PLB (Figure 1). $[\text{PLB}]_{\text{free}}$ is the unbound membrane concentration of PLB; $[\text{PLB}]_{\text{total}}$ is the calculated total membrane concentration of PLB, and $[\text{Ca-ATPase}]_{\text{total}}$ is the calculated total membrane concentration of the Ca-ATPase, which is 0.85 mM at a lipid-to-protein ratio of 750:1. At this lipid concentration, for reconstitution stoichiometries of PLB relative to the Ca-ATPase corresponding to 1:1, 4:1, and 11:1, $[\text{PLB}]_{\text{total}}$ equals 0.85, 3.4, and 9.4 mM and $[\text{PLB}]_{\text{free}}$ equals 0.26, 1.0, and 8.5 mM, respectively.

The dissociation constant (K_d) of PLB binding to the Ca-ATPase in the membrane can be determined by fitting the data to the Langmuir binding equation

$$Y = \frac{[\text{PLB}]_{\text{free}}}{K_d + [\text{PLB}]_{\text{free}}} \times \text{span} + \text{minimum} \quad (3)$$

where Y represents the dependent variable corresponding to either the fraction of nonexchangeable residues determined by ATR-FTIR or the shift in the calcium concentration associated with half-maximal activation of the Ca-ATPase (i.e., ΔK_{Ca}), span represents the dynamic range of the dependent variable, and minimum represents the value of the dependent variable in the absence of PLB.

Measurement of Free Calcium Concentrations. Free calcium concentrations were determined using the calcium sensitive fluorophore BAPTA ($\lambda_{\text{ex}} = 299$ nm, $\lambda_{\text{em}} = 360$ nm), as previously described (*35*). The dissociation constant for calcium binding to BAPTA was measured to be 203 ± 7 nM in a buffer containing 20 mM MOPS (pH 7.0), 0.1 M KCl, 5 mM $MgCl_2$, 5 mM ATP, 1 mM EGTA, and variable amounts of $CaCl_2$ prepared from desiccated $CaCO_3$ that was dissolved in 0.1 M HCl and adjusted to pH 7.0 with KOH.

Circular Dichroism Measurements. CD spectra were collected in a buffer containing 10 mM MOPS (pH 7.0) and 0.15 M sucrose at 20 °C using a Jasco J-710 spectropolarimeter (Jasco, Easton, MD) and a 0.05 cm path length quartz cell. Proteoliposomes containing the Ca-ATPase, PLB, or both proteins at different molar ratios have been prepared in three different reconstitution experiments, using previously described protocols that yield vesicles with an average diameter of 90 ± 7 nm (*36*). The CD spectra of each sample have been measured three or four times, and five scans were co-added in each measurement. Final CD spectra were obtained by averaging the spectra at each Ca-ATPase:PLB molar ratio, and the averaged data were smoothed using a 13-point Savitsky−Golay algorithm. Similar differences in CD spectra were observed irrespective of smoothing. The concentration of the Ca-ATPase was adjusted to 6.4 μM, and PLB was added to achieve the desired molar ratio of the two proteins.

The mean residue molar ellipticity, $[\theta]$, of the Ca-ATPase and PLB co-reconstituted in phospholipid vesicles was calculated using the following formula:

$$[\theta] = \frac{\theta_{\text{measured}} \times 10^{-3}}{([\text{P}_1]n_1 + [\text{P}_2]n_2)l} \quad (4)$$

where θ_{measured} is the measured ellipticity in millidegrees, $[P_1]$ and n_1 are the concentration (in decimoles per cubic centimeter) and the number of peptide bonds in the Ca-ATPase, respectively, $[P_2]$ and n_2 are those for PLB, respectively, and l is the path length of the CD cell. The molecular masses (M_r) and the number of peptide bonds were 110 458 and 1000, respectively, for the Ca-ATPase and 6093 and 52, respectively, for expressed [^{13}C]PLB.

Infrared Spectroscopic Measurements. Normally, ATR-FTIR measurements involved the acquisition of 1000 scans using a Magna-IR 560 infrared spectrometer (Nicolet Analytical Instruments, Madison, WI) at a nominal spectral resolution of 2 cm^{-1}, which were co-added to achieve the desired signal-to-noise ratio. For amide H/D exchange experiments, data for supported bilayers in H_2O buffer [10 mM HEPES (pH 7.4), 100 mM NaCl, and 0.1 mM $CaCl_2$] were first collected prior to flushing the cell with 10−12 volumes of D_2O buffer (pH* 7.0). The time point of first exposure of the reconstituted protein(s) to the D_2O buffer was taken to be the zero time point of H/D exchange. The time dependence of the amide H/D exchange was followed by recording 14 spectra during the first 8 h of exchange. In these experiments, the number of scans per spectrum was

gradually increased from 128 to 1000 and the time interval between successive spectra was correspondingly increased from 2 min to 2 h, taking into account the exponential nature of the kinetics of H/D exchange. The level of random noise in the spectra was estimated by the ESTNOISE program, included in the LabCalc software package, to be 0.01−0.03%. ATR-FTIR experiments, including measurements of amide H/D exchange kinetics, were repeated three times at each Ca-ATPase:PLB molar ratio.

The amide H/D exchange kinetics for proteins was determined on the basis of the analysis of the amide II band, as previously described (*37*). The amide II signal intensities were calculated by integrating the FTIR spectra between 1576 and 1532 cm^{-1} for the Ca-ATPase and between 1560 and 1515 cm^{-1} for [^{13}C]PLB. For co-reconstituted samples, the amide II region was decomposed into two components centered at approximately 1546 and 1525 cm^{-1} that correspond to the peaks of the second-derivative spectra. The areas of these components were normalized with respect to the corresponding amide II areas in H_2O and were used as integrated amide II intensities of the Ca-ATPase and [^{13}C]PLB. The fraction of nonexchanged amide protons (or "nonexchanged residues") was evaluated as

$$f(t) = \left(\frac{[H]}{[H] + [D]}\right)_t = \frac{(A_{amideII})_t}{(A_{amideII})_{t=0}} \quad (5)$$

and the time dependence of the amide H/D exchange was fit to the following multiexponential model:

$$f(t) = \left(\frac{[H]}{[H] + [D]}\right)_t = \sum_{i=1}^{n} \alpha_i e^{-t/\tau_i} \quad (6)$$

In this expression, n is the number of components associated with the exponential decay, t is a time point in the course of the H/D exchange, τ_i is the time constant, and α_i is the amplitude associated with each time constant. The goodness of fit was determined through a comparison of the deviations between the measured and calculated values.

The Gibbs free energies of amide H/D exchange were determined as described previously (*37*), using the following equation:

$$\Delta G = -RT \ln\left(\frac{\tau_o}{\tau_{obs}}\right) \quad (7)$$

where τ_o is the time constant of exchange for an unordered, completely solvent exposed residue and τ_{obs} is the time constant measured in the experiment. At 20 °C and pH* 7.0 (pD 7.4), $\tau_0 = 0.488$ s.

Second derivatives of FTIR spectra were used as a resolution enhancement method to reveal spectral features that are not readily visible in the raw spectra. Calculation of second derivatives was accompanied with 11-point Savitsky−Golay smoothing to eliminate high-frequency noise.

RESULTS

Functional Co-Reconstitution of the Ca-ATPase. PLB expressed and purified from *E. coli* was co-reconstituted with affinity-purified Ca-ATPase using lipids extracted from SR membranes, essentially as previously described (*29*, *38*). The fast twitch skeletal muscle SR Ca-ATPase (SERCA1) was used in these experiments because of (i) its greater stability in detergent compared with that of SERCA2a expressed in the cardiac SR and (ii) previous demonstrations that SERCA1 is fully regulated by PLB and can functionally substitute for SERCA2a in the heart (*7*, *8*, *26*, *39*). Irrespective of whether [^{12}C]PLB or [^{13}C]PLB was used for co-reconstitution with the Ca-ATPase, we find a similar activation of the Ca-ATPase for reconstituted and native cardiac preparations upon phosphorylation of PLB by PKA or increasing calcium concentrations (Figure 1). Thus, there is a 0.23 μM decrease in the calcium concentration associated with half-maximal activation of the Ca-ATPase (ΔK_{Ca}) upon phosphorylation of PLB both in native cardiac SR membranes and following co-reconstitution of the Ca-ATPase with PLB. Moreover, values of the maximal catalytic activity (i.e., V_{max}) for reconstituted vesicles are in good agreement with those for native SR membranes when differences in Ca-ATPase concentrations are taken into account. Using the formation of the phosphorylated intermediate to estimate the relative abundance of the Ca-ATPase, there are 2.0 ± 0.3 and 7.4 ± 0.4 nmol of Ca-ATPase/mg of total protein in native and reconstituted vesicles, respectively (*10*, *26*). Since the corresponding ATPase activities are 1.0 ± 0.1 and 4.0 ± 0.1 μmol of P_i mg^{-1} min^{-1}, it is apparent that the corresponding ATPase activities normalized to the abundance of the Ca-ATPase are approximately the same [i.e., 0.50 ± 0.09 and 0.54 ± 0.03 μmol of P_i per nmol of Ca-ATPase per min for native cardiac and reconstituted preparations, respectively]. Thus, the inhibitory interactions between PLB and the SERCA1 isoform of the Ca-ATPase in these reconstituted preparations are both qualitatively and quantitatively similar to those of SERCA2a in native cardiac SR membranes.

Addition of the calcium ionophore A23187 to either reconstituted vesicles or the native cardiac SR results in the same 2-fold stimulation of ATPase activity, indicating that reconstituted vesicles are tightly sealed. Detergent solubilization of reconstituted vesicles with $C_{12}E_9$ results in no further stimulation of activity relative to that induced by A23187. Thus, detergent solubilization only alters calcium permeability, and does not make additional catalytic sites of the Ca-ATPase available to substrates. These results indicate an asymmetrical reconstitution of the Ca-ATPase. In contrast, PLB is symmetrically reconstituted, as assessed by the ability to release approximately one-half of the cytosolic domain labeled with the fluorophore dansyl chloride. Thus, following exhaustive trypsin digestion, 44 ± 9% of the cytosolic portions of PLB (covalently modified with dansyl chloride) was released into the supernatant following reconstitution in either the absence or presence of the Ca-ATPase. Consistent with this result, the stoichiometry of PLB phosphorylation by PKA was measured to be 0.38 ± 0.08 mol of phosphate per mole of PLB. Thus, essentially all available sites on PLB are phosphorylated by PKA. These results, coupled with the fact that the extent of regulation following co-reconstitution of PLB with the Ca-ATPase is equivalent to that with native cardiac SR vesicles, indicate a preferential association between Ca-ATPase and PLB molecules whose cytosolic domain faces the vesicle exterior.

Circular Dichroism Assessment of the Structural Interaction between PLB and the Ca-ATPase. To characterize the

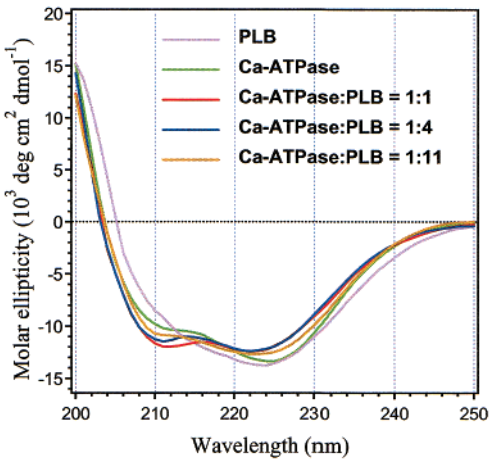

FIGURE 2: Circular dichroism spectra of [^{13}C]PLB, the Ca-ATPase, and following co-reconstitution of the Ca-ATPase with [^{13}C]PLB at different molar ratios, as indicated. Each spectrum represents the average of three or four spectra of different (co-)reconstituted samples, each of which was recorded by co-adding five scans. Measurements were made in 10 mM MOPS (pH 7.0) and 0.15 M sucrose at 20 °C.

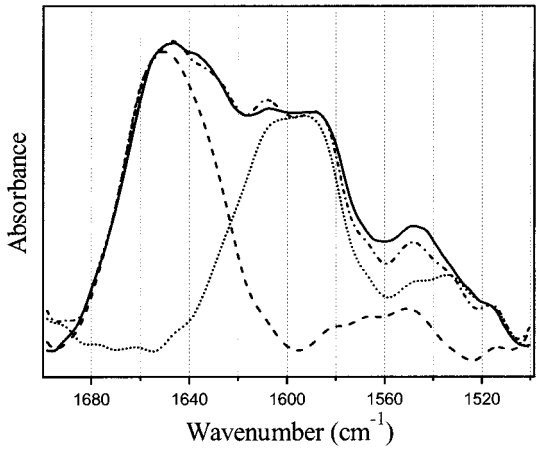

FIGURE 3: ATR-FTIR spectra of the Ca-ATPase (- - -), [^{13}C]PLB (•••), following co-reconstitution of the Ca-ATPase with an 11-fold molar excess of [^{13}C]PLB (—), and following summation of the individual spectra of the Ca-ATPase and [^{13}C]PLB (-•-). In the case of the Ca-ATPase, the amide I and II components are centered near 1658 and 1546 cm^{-1}, respectively. In the case of [^{13}C]PLB, the amide I band contains two spectral components centered at 1608 and 1585 cm^{-1} while the amide II component is centered near 1525 cm^{-1}.

secondary structures of PLB and the Ca-ATPase, and to assess the structural effects accompanying the interaction between PLB and the Ca-ATPase, CD spectra were measured using proteoliposomes containing PLB and the Ca-ATPase, or following co-reconstitution of these integral membrane proteins (Figure 2). The shape of the CD spectrum of [^{13}C]PLB deviates from a typical α-helical spectrum. In particular, the $\pi-\pi^*$ parallel transition, which is normally observed near 208 nm as a local minimum for an α-helix, is only present as a shoulder in the CD spectrum of PLB. While the amount of β-structure cannot be reliably estimated from CD data collected above 200 nm, these results suggest the presence of β-structure in PLB (*40*, *41*). In contrast, the CD spectrum for the Ca-ATPase contains two clearly resolved minima centered near 208 and 222 nm indicating that the secondary structure of the protein is dominated by α-helices. This is consistent with earlier CD measurements as well as the recently determined crystal structure of the Ca-ATPase (*40*, *42*−*45*).

The spectrum of the Ca-ATPase and PLB following their co-reconstitution is not simply a weighted average of the spectra of either protein separately reconstituted into lipid vesicles. In particular, the ratio of molar ellipticities centered near 208 nm ($\pi-\pi^*$ parallel transition) and 222 nm ($n-\pi^*$ transition) (i.e., $[\theta]_{208}/[\theta]_{222}$) increases following co-reconstitution. The small diameter of the vesicles (90 ± 7 nm) ensures that the observed differences are not due to either differential scattering or absorption flattening artifacts (*46*). Therefore, the CD data suggest that the interaction between the Ca-ATPase and PLB is accompanied by conformational changes in either one protein or both proteins. Spectral overlap of the CD spectra associated with both PLB and the Ca-ATPase prevents a quantitative interpretation of these results in terms of changes in the relative fractions of secondary structural elements. However, an increase in $[\theta]_{208}/[\theta]_{222}$ is conventionally interpreted in terms of secondary structural changes involving a transition from less stable α-helical structures, including helical coiled coils, to α-helices with increased rigidity (*40*, *47*−*50*). Thus, co-reconstitution of the Ca-ATPase and PLB may weaken or abolish interhelical interactions within either protein, resulting in a transition from flexible coiled-coil superhelices to normal, more rigid helices.

Spectral Resolution of the Ca-ATPase and Phospholamban by ATR-FTIR Spectroscopy. Additional resolution of secondary structural changes is possible using infrared spectroscopy (*19*). Isotopic labeling of PLB with ^{13}C induces a substantial shift of both the amide I and II bands toward lower frequencies, permitting the spectral resolution of the infrared spectra of unlabeled Ca-ATPase from ^{13}C-labeled PLB (Figure 3). In the case of the Ca-ATPase, the amide I and II components are centered near 1658 and 1546 cm^{-1}. In the case of [^{13}C]PLB, the amide I component contains two spectral components centered at 1608 and 1585 cm^{-1}, while the amide II component is centered near 1525 cm^{-1}. Comparison of the experimental spectrum obtained following co-reconstitution of the Ca-ATPase with [^{13}C]PLB with the sum of the spectra obtained for each protein reconstituted separately indicates that there are no significant differences in the amide I spectral regions of either the Ca-ATPase or PLB (Figure 3). Likewise, the spectral intensity near 1525 cm^{-1} corresponding to the amide II band of [^{13}C]PLB is unchanged following co-reconstitution of the Ca-ATPase with [^{13}C]PLB. In contrast, spectral intensity differences are apparent near 1546 cm^{-1} following co-reconstitution of the Ca-ATPase with [^{13}C]PLB, which corresponds to the amide II band of the Ca-ATPase. These intensity differences between the spectrum obtained following co-reconstitution of the Ca-ATPase with PLB and the composite spectrum obtained by mathematically summing the individual spectra of PLB and the Ca-ATPase suggest that there are structural changes involving the Ca-ATPase (apparent in the amide II region) following co-reconstitution with PLB.

The 20 cm^{-1} shift of the amide II band of PLB (from approximately 1545 to 1525 cm^{-1}) following ^{13}C labeling is smaller than that of the amide I band (see below) because the backbone carbonyl carbon atom contributes less to the amide II mode than it does to the amide I vibration. The amide I mode of ^{13}C-labeled PLB results in a broad band

that incorporates two spectral components centered near 1608 and 1585 cm^{-1}, as evidenced by the second-derivative spectra (data not shown). The component at ~1608 cm^{-1} represents the amide I band of α-helical elements in PLB, which is shifted toward lower frequencies by approximately 50 cm^{-1} due to ^{13}C labeling. This effect is due to the heavier nuclear mass of ^{13}C relative to that of ^{12}C, and is consistent with the 45−55 cm^{-1} spectral shift in the amide I band detected in other ^{13}C-labeled proteins by transmission FTIR spectroscopy (*20*, *21*). The component at ~1585 cm^{-1} corresponds to the amide I mode of secondary structural elements of a ^{13}C-labeled protein that assume a *β*-conformation (*51*−*53*). This spectral component corresponds to approximately 30% of the spectral intensity within the amide I band and provides an estimate of the amount of *β*-structure in PLB. Since certain unlabeled side chains such as Arg, Asn, Asp, Gln, and Glu also absorb in this spectral region and contribute to the component near 1585 cm^{-1}, this result suggests that the spectral intensity measured at 1585 cm^{-1} is the upper limit with respect to the fractional contribution of *β*-structure (*54*−*56*). However, complete isotopic incorporation of ^{13}C is indicated by the lack of any residual absorption in the amide I regions of the unlabeled protein (i.e., near 1650 cm^{-1}). Thus, both the ATR-FTIR and CD data (see above) suggest a considerable fraction of *β*-structure in PLB.

Conformational Changes Resulting from the Interaction between PLB and the Ca-ATPase. To characterize possible conformational changes within either the Ca-ATPase or PLB resulting from their interaction, we compared the ATR-FTIR spectra of the Ca-ATPase and [^{13}C]PLB individually reconstituted into lipid bilayers with the spectrum obtained following co-reconstitution of the two proteins (Figure 3). Resolution enhancement techniques, such as Fourier self-deconvolution or derivatization, are conventionally used to identify the spectral features (e.g., shoulders) that are not readily visible in the absorbance spectrum (*19*). The inverted second-derivative spectra of the Ca-ATPase in the absence and presence of PLB at different time points of amide deuteration, presented in Figure 4, provide valuable information about how interaction with PLB affects both the secondary and dynamic structures of the Ca-ATPase. (The use of *inverted* second derivatives reveals the features of the amide I band in a more straightforward way because, in this case, the peaks, not the dips, correspond to amide I band components.) Thus, second-derivative spectral peaks allow resolution of individual bands in the amide I region that correspond to both protonated and deuterated signals for each protein secondary structural element (e.g., 1658 and 1647 cm^{-1} are associated respectively with protonated and deuterated α-helices) (Figure 4). Spectral features that are identified include turns (1700−1670 cm^{-1}), *β*-sheets (1637−1625 cm^{-1}), and α-helices (1658−1647 cm^{-1}). In addition, features corresponding to certain side chains containing amide groups or aromatic rings are visible in the second-derivative spectra in the region between 1605 and 1610 cm^{-1}.

One of the most salient spectral features observed upon co-reconstitution with PLB is a reproducible shift in the absorbance peak of the Ca-ATPase from 1658.5 to 1655.0 cm^{-1}, corresponding to α-helices. Lower-frequency α-helical components of amide I bands are thought to result from more stable α-helices that are characterized by stronger H-bonding (*57*−*60*). This suggestion follows from the fact that the amide I band is mainly generated by the backbone carbonyl stretching vibrations of the polypeptide chain, and the vibrational frequency is proportional to the square root of the bond strength. This indicates that the main chain carbonyl bonds within α-helices of the Ca-ATPase become weaker due to strengthening of helical H-bonding upon interaction with PLB. Therefore, this finding suggests that interaction of the Ca-ATPase with PLB results in a stabilization of the α-helices in the Ca-ATPase.

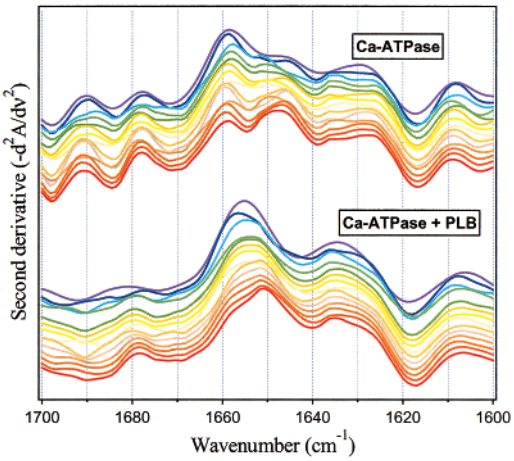

FIGURE 4: Second-derivative ATR-FTIR spectra of the amide I band of the Ca-ATPase reconstituted in the absence (top family of curves) and presence (bottom family of curves) of an equal molar concentration of [^{13}C]PLB. The change in the color code from blue to red corresponds to an increase in the time of deuteration from 2 min to 8 h. Spectra are inverted and offset to permit visualization of spectral changes that occur during H/D exchange, and from top to bottom correspond to exchange times of 2 min, 4 min, 9 min, 14 min, 19 min, 26 min, 36 min, 1 h, 1.4 h, 2.3 h, 3 h, 4.4 h, 6 h, and 8 h.

Consistent with this result, the presence of PLB results in a reduction in the rate of amide H/D exchange of the Ca-ATPase. This is apparent in the second-derivative spectra of the Ca-ATPase in the absence of PLB, where a component at ~1647 cm^{-1} generated by deuterated α-helices is already present in the earliest spectrum corresponding to 2 min of H/D exchange, and gradually increases over the course of deuteration (Figure 4). In comparison, amide H/D exchange of the Ca-ATPase reconstituted with PLB results in a smaller spectral shift (from ~1655 to ~1651 cm^{-1}) and is much slower. These results suggest that the inhibitory association of PLB with the Ca-ATPase involves an increase in the rigidity of selected α-helices within the Ca-ATPase. Besides this major effect, changes in the spectrum of the Ca-ATPase following co-reconstitution with PLB are detected in other regions of the amide I band, corresponding to turn (1700−1670 cm^{-1}) and *β*-structures (1637−1625 cm^{-1}). In the spectrum of the Ca-ATPase with PLB, the relative population of unexchanged *β*-structures (~1636 cm^{-1}) is considerably larger than that of the deuterated *β*-structure (~1625 cm^{-1}), while in the absence of PLB these two components are nearly equally populated. This result is consistent with a stabilizing effect of PLB on the secondary structure of the Ca-ATPase, which is further confirmed by the analysis of the amide II band of the Ca-ATPase reconstituted with and without PLB.

Amide H/D Exchange Measurements. Amide H/D exchange causes a shift of the amide II band from ~1545 to ~1450 cm^{-1}, thus resulting in a progressive reduction in the

Table 1: H/D Exchange Parameters for the Ca-ATPase and [^{13}C]PLB Determined Using ATR-FTIR[a]

H/D exchange parameter	Ca-ATPase				[^{13}C]PLB	
	1:0[b]	1:1[b]	1:4[b]	1:11[b]	0:1[b]	1:11[b]
α_1	0.39 ± 0.02	0.33 ± 0.01*	0.31 ± 0.02*	0.29 ± 0.01*	0.38 ± 0.01	0.48 ± 0.01*
τ_1 (min)	1.0 ± 0.1	0.9 ± 0.2	0.9 ± 0.1	0.8 ± 0.1	1.6 ± 0.2	1.5 ± 0.3
ΔG_1 (kcal/mol)	2.8 ± 0.1	2.7 ± 0.1	2.7 ± 0.1	2.7 ± 0.1	3.1 ± 0.1	3.0 ± 0.1
α_2	0.39 ± 0.02	0.38 ± 0.03	0.38 ± 0.03	0.40 ± 0.01	0.33 ± 0.01	0.27 ± 0.02
τ_2 (min)	57 ± 6	78 ± 9*	75 ± 5*	77 ± 6*	63 ± 6	90 ± 20*
ΔG_2 (kcal/mol)	5.16 ± 0.06	5.34 ± 0.04	5.31 ± 0.04	5.33 ± 0.05	5.21 ± 0.06	5.42 ± 0.14
A_∞	0.22 ± 0.01	0.28 ± 0.02*	0.29 ± 0.02*	0.31 ± 0.01*	0.29 ± 0.01	0.25 ± 0.01*

[a] Asterisks indicate statistically significant changes relative to the single-component system determined using the Student's *t* test ($p = 0.05$). H/D exchange parameters represent the average and standard errors of the mean for three independent measurements, and were obtained from a least-squares fit using eqs 6 and 7 in Materials and Methods. [b] Ca-ATPase:PLB molar ratio.

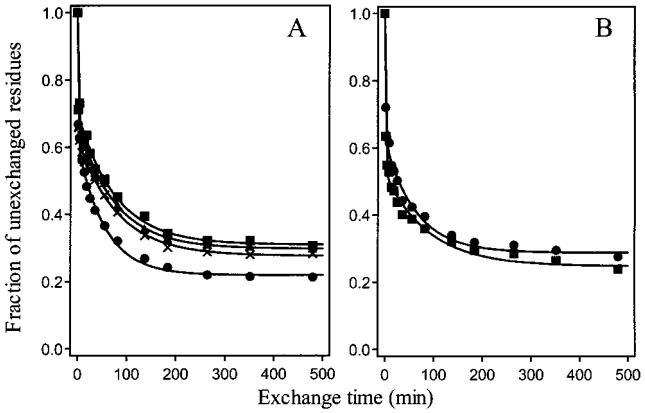

FIGURE 5: Time course of H/D exchange of (A) the Ca-ATPase reconstituted in the absence (●) or presence of 1:1 (×), 4:1 (▲), and 11:1 PLB:Ca-ATPase molar ratios (■) or (B) [^{13}C]PLB reconstituted in the absence (●) or presence (■) of the Ca-ATPase at a PLB:Ca-ATPase molar ratio of 11:1. Fractions of unexchanged residues represent the normalized areas associated with the amide II band of the Ca-ATPase (between 1576 and 1532 cm^{-1}) and [^{13}C]PLB (between 1560 and 1515 cm^{-1}) for spectra obtained at the indicated times of H/D exchange, as described in Materials and Methods. The curves represent the nonlinear least-squares fit to eq 6 ($n = 3$), and the best fit parameters are summarized in Table 1.

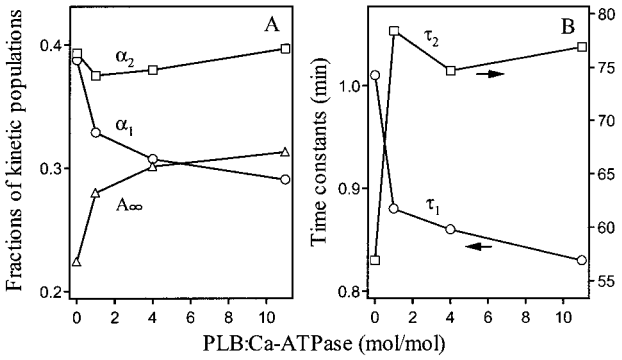

FIGURE 6: Dependence of the amplitudes (A) and time constants (B) of amide H/D exchange of the Ca-ATPase on the PLB:Ca-ATPase molar ratio. Data points correspond to populations of residues undergoing fast exchange (○), residues undergoing slow exchange (□), and those that are exchange resistant (△). In panel B, the arrows indicate that the left (right) vertical axis applies to τ_1 (τ_2). Average data and associated standard deviations are summarized in Table 1.

intensity at ~1545 cm^{-1}. The results indicate that the spectra of the Ca-ATPase co-reconstituted with PLB exhibit stronger unexchanged amide II bands than the corresponding spectra in the absence of PLB (Figure 3). These data imply a decrease in the efficiency of amide H/D exchange of the Ca-ATPase upon interaction with PLB, and provide additional evidence for the stabilization of the structure of the Ca-ATPase by PLB. The measurements of amide H/D exchange were carried out at saturating calcium concentrations to ensure that there was no time-dependent inactivation of the Ca-ATPase during the time course of the experiment. Description of the data using a multiexponential function indicates a substantial decrease in the extent of H/D exchange following co-reconstitution of the Ca-ATPase with PLB (Figure 5A). The kinetics of H/D exchange demonstrates the presence of three populations (Table 1), which undergo fast exchange (α_1 and τ_1), undergo slow exchange (α_2 and τ_2), and are H/D exchange resistant (A_∞). The calculated Gibbs free energy of the fast exchange process (i.e., $\Delta G \approx 3$ kcal/mol) is similar to that associated with amide hydrogen bonding in water, suggesting that these residues probably belong to solvent-exposed secondary structures. Thus, the population of fast exchanging residues is likely to involve α-helices and β-sheets of the cytoplasmic domains of the Ca-ATPase, as well as the residues of the transmembrane helices lining the water-filled crevice that contains the calcium ligands (*45*).

Co-reconstitution with increasing amounts of PLB results in a progressive decrease in the fraction of fast exchanging residues (α_1) with a corresponding increase in the fraction of H/D exchange resistant residues (A_∞) of the Ca-ATPase, while no significant changes in the fraction of slow exchanging residues (α_2) are detected (Figure 6A). Also, the time constant of fast exchanging residues (τ_1) slightly decreases, and that of the slow exchanging residues (τ_2) significantly increases (Figure 6B). Since the SERCA1 isoform of the Ca-ATPase contains 1001 amino acids, PLB association with the Ca-ATPase decreases the fraction of fast exchanging residues from 390 ± 20 to 290 ± 10 with a corresponding increase in the fraction of H/D exchange resistant residues in the Ca-ATPase from 220 ± 10 to 310 ± 10 amino acids. Thus, PLB stabilizes the secondary structure of the Ca-ATPase and decreases the solvent accessibility of the protein interior, resulting in a decreased efficiency of H/D exchange. These structural changes are consistent with large-scale domain reorientations in the Ca-ATPase previously detected using spin-label EPR and phosphorescence anisotropy (*10*, *18*, *61*). PLB undergoes more moderate changes in its H/D exchange characteristics upon interaction with the Ca-ATPase, as reflected in an increase in the fraction of fast exchanging residues and a decrease in the number of residues that undergo slower exchange or are H/D exchange resistant (Figure 5B and Table 1), which might result from steric

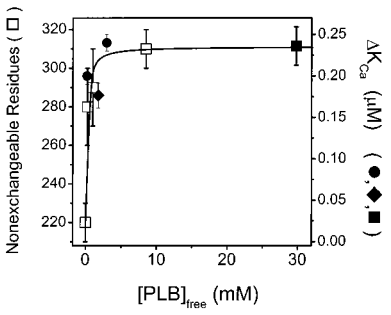

FIGURE 7: PLB concentration dependence of the number of Ca-ATPase residues that are resistant to H/D exchange (□) or the shift in the half-point of the calcium dependence of ATP hydrolysis activity (ΔK_{Ca}) for reconstituted samples (●) or using proteoliposomes isolated from either soleus (◆) or cardiac (■) muscle. The PLB:Ca-ATPase molar ratios for co-reconstituted samples used for the ATR-FTIR measurements of H/D exchange were 1:1, 4:1, and 11:1 (□). The PLB:Ca-ATPase molar ratio for co-reconstituted samples used for the determination of ΔK_{Ca} were 1:1 and 3:1 (●). The PLB:Ca-ATPase molar ratios in vesicles made from soleus (◆) and cardiac (■) muscle were 1:1 and 6:1, respectively. The line was constructed according to eq 3, and represents a nonlinear least-squares fit to all of the data, where $K_d = 140 \pm 30$ μM as determined from a global fit to both data sets. For the ATR-FTIR and activity measurements, span was determined to equal 87 ± 5 residues and 0.22 ± 0.01 μM calcium, respectively. For the ATR-FTIR and activity measurements, minimum was determined to equal 220 ± 3 residues or 0.01 ± 0.01 μM calcium, respectively. Activity data are taken from ref *62*.

effects related to Ca-ATPase-induced depolymerization of PLB (*15*).

The dependence of H/D exchange on the ratio of PLB incorporated into the reconstituted vesicles demonstrates that the effect of PLB on the fractions of H/D exchange resistant (A_∞) and fast exchanging (α_1) residues of the Ca-ATPase is 70 ± 6% saturated at an equimolar stoichiometry of the Ca-ATPase and PLB (Figure 6A). This is similar to our earlier finding indicating that approximately 70% of the maximal inhibitory effect on Ca-ATPase activity was observed following co-reconstitution of the Ca-ATPase with an equimolar amount of PLB (*29*, *62*). These results suggest that a single PLB molecule exerts the primary effect on observed functional and secondary structural changes of the Ca-ATPase (*8*, *63*). The specificity of this interaction is, furthermore, apparent from a consideration of the concentration dependence of the structural interaction and associated inhibition of the Ca-ATPase by PLB (Figure 7). Knowledge of the lipid-to-protein ratio and the molar ratio of the Ca-ATPase and PLB permits an estimation of their molar concentration, as discussed in Materials and Methods. Following correction for the concentration of PLB bound to the Ca-ATPase, one can determine the binding isotherm associated with either the structural interaction between the Ca-ATPase and PLB measured by ATR-FTIR or that associated with the functional inhibition (Figure 7). It should be noted that the calculation of the unbound concentration of PLB corrects for differences in the lipid-to-protein ratio associated with reconstituted and native vesicles, whose respective lipid-to-protein ratios are approximately 750:1 and 100:1. It is apparent that there is a similar dependence on PLB concentration for both the fraction of H/D exchange resistant residues in the Ca-ATPase (A_∞; Table 1) and the functional inhibition of the Ca-ATPase (ΔK_{Ca}). Thus, the observed alterations in the H/D exchange kinetics of the Ca-ATPase measured by ATR-FTIR reflect the structural interactions responsible for the functional inhibition of the Ca-ATPase. Furthermore, by simultaneously fitting both data sets to a Langmuir binding isotherm (described in Materials and Methods), we were able to estimate the dissociation constant (K_d) for PLB binding to the Ca-ATPase, which is 140 ± 30 μM irrespective of the presence of saturating concentrations of calcium.

DISCUSSION

Summary of Results. Previous structural measurements of PLB or the Ca-ATPase using either infrared or CD spectroscopy have involved single-component systems (*30*, *42*, *64*−*67*). This has prevented an assessment of the secondary structure of the functional form of PLB in association with the Ca-ATPase. Moreover, no prior evidence has been available regarding possible changes in the secondary structure of the Ca-ATPase induced by association with PLB that may be important to its functional regulation. The use of isotopic labeling strategies and fully functional reconstitution procedures permits the resolution of the amide I and II absorption bands of both the Ca-ATPase and [^{13}C]PLB, which, in turn, allows the measurement of secondary and dynamic structural changes resulting from the inhibition of the Ca-ATPase by PLB. Conformational alterations involving the stabilization of α-helices in the Ca-ATPase resulting from its interaction with PLB were detected by both CD and ATR-FTIR spectroscopy. The dependence of the observed alterations of H/D exchange kinetics on PLB concentration is virtually identical to that associated with the functional inhibition of the Ca-ATPase (Figure 7), indicating that the observed structural changes are functionally relevant. Furthermore, 60−70% of the reduction in fast exchanging residues within the Ca-ATPase is apparent when equimolar amounts of PLB are co-reconstituted with the Ca-ATPase, which are characterized by a single binding site with a dissociation constant of 140 ± 30 μM (Figures 6 and 7). These results support earlier suggestions that the monomeric form of PLB represents the inhibitory species (*8*, *63*), and suggest that PLB inhibits Ca-ATPase function by restricting catalytically important motional flexibility of the enzyme.

Secondary Structural Measurements of PLB. While no previous measurements have investigated the secondary structure of PLB in association with the Ca-ATPase, it is of interest to compare the present measurements with earlier estimates of the secondary structure of PLB. Previous CD measurements of PLB purified from the canine cardiac SR indicated that PLB contained between 68 and 74% α-helix and between 2 and 11% β-structure, depending on the detergent and co-solvent (*64*, *68*). Similar results were obtained using ATR-FTIR spectroscopy to investigate the secondary structure of a recombinant PLB reconstituted in lipid bilayers, which suggested the presence of between 64 and 67% α-helix and between 9 and 11% β-structure (*30*). In contrast, FTIR measurements of a synthesized PLB reported a much higher α-helical content and essentially no β-structure (*66*). In a recent NMR study, the structure of a synthetic PLB mutant (C41F) dissolved in a mixture of chloroform and methanol was found to contain two α-helices (residues 4−16 and 22−49, which comprise 79% of all residues) connected by a flexible β-turn (*69*). In the current study, CD and ATR-FTIR measurements of [^{13}C]PLB revealed the presence of both α-helical and β-structure

(Figures 2 and 3). These results strongly support the majority of earlier suggestions that PLB contains β-structure.

Secondary Structural Measurements of the Ca-ATPase. Earlier secondary structural measurements of the Ca-ATPase are in general agreement with the recently determined atomic resolution crystal structure of the Ca-ATPase, which indicates that the Ca-ATPase contains 39% α-helix, 14% β-strand, 14% turns, 2% 3_{10}-helix, and 30% irregular structure (*45*). For comparison, previous CD, FTIR, and Raman spectroscopy measurements of the Ca-ATPase indicated the presence of 40−50% α-helix, 7−26% β-sheet, 13−30% β-turn, and up to 35% irregular structure (*43*, *65*, *70*). While the content of α-helix was not affected by detergent solubilization, estimates of β-sheet content increased from 7 to 26% (*43*), suggesting that the secondary structure of the Ca-ATPase is sensitive to the surrounding lipid microenvironment. Therefore, the recently determined crystal structure of the detergent-solubilized Ca-ATPase may not precisely reflect that of the membrane-bound protein. These latter results are consistent with earlier phosphorescence anisotropy measurements in which catalytically important motions involving the nucleotide binding domain were shown to be affected by alterations in the phospholipid composition of the membrane that correlate with transport function (*36*, *71*). Thus, dynamic structural alterations involving secondary and tertiary structural changes of the Ca-ATPase are sensitive to specific interactions with regulators of transport function.

Structural Coupling between PLB and the Ca-ATPase. The ATR-FTIR spectra indicate stabilization of α-helical components of the Ca-ATPase following its functional association with PLB. This is apparent from (i) the observed spectral shifts in the amide I absorbance band, (ii) corresponding reductions in the fraction of residues undergoing rapid H/D exchange, and (iii) an increase in the number of exchange resistant residues of the Ca-ATPase upon association with PLB. There are no corresponding large changes in the secondary structure of PLB upon association with the Ca-ATPase. While no prior reports have addressed possible secondary structural changes that may underlie the functional inhibition of the Ca-ATPase by PLB, prior spin-label EPR and phosphorescence anisotropy measurements indicate that PLB restricts the amplitude of catalytically important domain motions involving the nucleotide binding domain that is implicated in the calcium-dependent utilization of nucleotide (*10*, *72*). In contrast, calcium activation was shown to increase the amplitude of motion associated with the nucleotide binding domain to facilitate nucleotide utilization (*73*). Thus, PLB binding increases the activation barrier associated with conformational changes coupled to calcium activation by stabilizing α-helical secondary structural elements within the Ca-ATPase. These results are in agreement with earlier observations that PLB does not alter equilibrium calcium binding to the Ca-ATPase, but rather increases the activation barrier associated with calcium activation and nucleotide utilization (*9*, *10*).

Proposed Mechanism of Inhibition of the Ca-ATPase by PLB. We have demonstrated that the inhibitory effect of PLB on Ca-ATPase transport function involves the stabilization of α-helices within the Ca-ATPase, which results in a more rigid structure. In contrast, PLB undergoes relatively modest structural changes upon interaction with the Ca-ATPase that are consistent with steric effects arising from depolymerization upon interaction with the Ca-ATPase (*15*). These results in the context of prior measurements involving site-directed mutagenesis, and knowledge of the recently determined high-resolution structures of PLB and the Ca-ATPase, suggest possible mechanisms associated with the functional inhibition of the Ca-ATPase by PLB. Previously, two sites have been identified in the Ca-ATPase that are involved in mediating the association with PLB, namely, residues Val^{795}, Leu^{802}, Thr^{805}, and Phe^{809} located on one face of the M6 transmembrane helix (Val^{790}−Phe^{809}) of the Ca-ATPase and the sequence of Lys^{397}−Arg^{403} in the nucleotide binding domain. These sites have been suggested to interact with the transmembrane and cytoplasmic domains of PLB, respectively (*7*, *8*, *11*, *14*, *39*, *74*). Furthermore, PLB has been demonstrated to readily self-associate through contacts between transmembrane helices (*75*, *76*). We, therefore, propose that the sequence similarity between the inverted sequence of the transmembrane helix of PLB and the sequence of the M6 helix of the Ca-ATPase may facilitate the interaction between PLB and the Ca-ATPase. In fact, the sequence Leu^{792}-Leu-Trp-Val-Asn-Leu-Val-Thr-Asp-Gly-Leu-Pro-Ala-Thr-Ala-Leu-Gly-Phe^{809} of the Ca-ATPase can be aligned with the inverted sequence of PLB (Leu^{52}-Leu-Met-Val-Ile-Ile-Cys-Ile-Leu-Leu-Leu-Cys-Ile-Leu-Ile-Leu-Cys-Phe^{35}) to yield a level of sequence identity of 33%. This alignment would provide an efficient network of leucine−isoleucine zipper type interactions between the M6 transmembrane helix of the Ca-ATPase and PLB. Additional interactions between PLB are possible with other transmembrane helices of the Ca-ATPase, including M4 which provides the majority of the ligands to calcium-binding site II (*45*). The transmembrane helices in both M4 or M6 are distorted in the middle of the membrane-spanning sequence to provide the necessary flexibility to permit backbone or side chain oxygens to efficiently coordinate two calcium ions. Therefore, PLB binding to either M4 or M6 would be expected to restrict the dynamics of these sequences, which is consistent with the increase in the energy barrier associated with calcium activation and the observed reduction in the level of Ca-ATPase function (*9*, *10*, *18*). In this respect, it is notable that PLB restricts the amplitude of catalytically important motions involving the nucleotide binding domain normally coupled to calcium activation, which are associated with nucleotide utilization and the formation of the phosphorylated intermediate (*18*, *73*). These results suggest that PLB inhibits calcium transport by stabilizing α-helical elements to rigidify the Ca-ATPase and diminish transport function.

REFERENCES

1. Kranias, E. G. (1985) *J. Biol. Chem. 260*, 11006−11010.
2. Simmerman, H. K., Collins, J. H., Theibert, J. L., Wegener, A. D., and Jones, L. R. (1986) *J. Biol. Chem. 261*, 13333−13341.
3. Tada, M., Kadoma, M., Inui, M., and Fujii, J. (1988) *Methods Enzymol. 157*, 107−154.
4. Jones, L. R., Wegener, A. D., and Simmerman, H. K. (1988) *Methods Enzymol. 157*, 360−369.
5. Simmerman, H. K., and Jones, L. R. (1998) *Physiol. Rev. 78*, 921−947.
6. Sasaki, T., Inui, M., Kimura, Y., Kuzuya, T., and Tada, M. (1992) *J. Biol. Chem. 267*, 1674−1679.
7. Toyofuku, T., Kurzydlowski, K., Tada, M., and MacLennan, D. H. (1994) *J. Biol. Chem. 269*, 3088−3094.

8. Toyofuku, T., Kurzydlowski, K., Tada, M., and MacLennan, D. H. (1994) *J. Biol. Chem. 269*, 22929−22932.
9. Cantilina, T., Sagara, Y., Inesi, G., and Jones, L. R. (1993) *J. Biol. Chem. 268*, 17018−17025.
10. Negash, S., Chen, L. T., Bigelow, D. J., and Squier, T. C. (1996) *Biochemistry 35*, 11247−11259.
11. Asahi, M., Kimura, Y., Kurzidlowski, K., Tada, M., and MacLennan, D. H. (1999) *J. Biol. Chem. 274*, 32855−32862.
12. James, P., Inui, M., Tada, M., Chiesi, M., and Carafoli, E. (1989) *Nature 342*, 90−92.
13. MacLennan, D. H., Kimura, Y., and Toyofuku, T. (1998) *Ann. N.Y. Acad. Sci. 853*, 31−42.
14. Kimura, Y., Kurzydlowski, K., Tada, M., and MacLennan, D. H. (1996) *J. Biol. Chem. 271*, 21726−21731.
15. Reddy, L. G., Jones, L. R., and Thomas, D. D. (1999) *Biochemistry 38*, 3954−3962.
16. Chen, L., Yao, Q., Brungardt, K., Squier, T., and Bigelow, D. (1998) *Ann. N.Y. Acad. Sci. 853*, 264−266.
17. Thomas, D. D., Reddy, L. G., Karim, C. B., Cornea, R., Autry, J. M., Jones, L. R., and Stamm, J. (1998) *Ann. N.Y. Acad. Sci. 853*, 186−194.
18. Negash, S., Huang, S., and Squier, T. C. (1999) *Biochemistry 38*, 8150−8158.
19. Tamm, L. K., and Tatulian, S. A. (1997) *Q. Rev. Biophys. 30*, 365−429.
20. Haris, P. I., Robillard, G. T., van Dijk, A. A., and Chapman, D. (1992) *Biochemistry 31*, 6279−6284.
21. Zhang, M., Fabian, H., Mantsch, H. H., and Vogel, H. J. (1994) *Biochemistry 33*, 10883−10888.
22. Fernandez, J. L., Rosemblatt, M., and Hidalgo, C. (1980) *Biochim. Biophys. Acta 599*, 552−568.
23. Chen, P. S., Toribara, T. Y., and Warner, H. (1956) *Anal. Chem. 28*, 1756−1758.
24. Hidalgo, C., Ikemoto, N., and Gergely, J. (1976) *J. Biol. Chem. 251*, 4224−4232.
25. Coll, R. J., and Murphy, A. J. (1984) *J. Biol. Chem. 259*, 14249−14254.
26. Yao, Q., Chen, L. T., and Bigelow, D. J. (1998) *Protein Expression Purif. 13*, 191−197.
27. Yao, Q., Bevan, J. L., Weaver, R. F., and Bigelow, D. J. (1996) *Protein Expression Purif. 8*, 463−468.
28. Lévy, D., Gulik, A., Bluzat, A., and Rigaud, J.-L. (1992) *Biochim. Biophys. Acta 1107*, 283−298.
29. Reddy, L. G., Jones, L. R., Cala, S. E., O'Brian, J. J., Tatulian, S. A., and Stokes, D. L. (1995) *J. Biol. Chem. 270*, 9390−9397.
30. Tatulian, S. A., Jones, L. R., Reddy, L. G., Stokes, D. L., and Tamm, L. K. (1995) *Biochemistry 34*, 4448−4456.
31. Lanzetta, P. A., Alvarez, L. J., Reinach, P. S., and Candia, O. A. (1979) *Anal. Biochem. 100*, 95−97.
32. Schaffner, W., and Weissmann, C. A. (1973) *Anal. Biochem. 56*, 502−514.
33. Haugland, R. (1996) *Handbook of Fluorescent Probes and Research Chemicals*, Molecular Probes, Eugene, OR.
34. Pedigo, S., and Shea, M. A. (1995) *Biochemistry 34*, 10676−10689.
35. Swenson, C. A., and Fredricksen, R. S. (1992) *Biochemistry 31*, 3420−3429.
36. Hunter, G. W., Negash, S., and Squier, T. C. (1999) *Biochemistry 38*, 1356−1364.
37. Tatulian, S. A., Cortes, D. M., and Perozo, E. (1998) *FEBS Lett. 423*, 205−212.
38. Szimańska, G. H., Kim, W., Cuppoletti, J., and Kranias, E. G. (1990) *Membr. Biochem. 9*, 191−202.
39. Toyofuku, T., Kurzydlowski, K., Tada, M., and MacLennan, D. H. (1993) *J. Biol. Chem. 268*, 2809−2815.
40. Fasman, G. D. (1996) in *Circular Dichroism and the Conformational Analysis of Biomolecules* (Fasman, G. D., Ed.) pp 381−412, Plenum Press, New York.
41. Kelly, S. M., and Price, N. C. (1997) *Biochim. Biophys. Acta 1338*, 161−185.
42. Nakamoto, R. K., and Inesi, G. (1986) *FEBS Lett. 194*, 258−262.
43. Csermely, P., Katopis, C., Wallace, B. A., and Martonosi, A. (1987) *Biochem. J. 241*, 663−669.
44. Chen, B., Jones, T. E., and Bigelow, D. J. (1999) *Biochemistry 38*, 14887−14896.
45. Toyoshima, C., Nakasako, M., Nomura, H., and Ogawa, H. (2000) *Nature 405*, 647−655.
46. Glaeser, R. M., and Jap, B. K. (1985) *Biochemistry 24*, 6398−6401.
47. Manning, M. C., Illangasekare, M., and Woody, R. W. (1988) *Biophys. Chem. 31*, 77−86.
48. Gibson, N. J., and Cassim, J. Y. (1989) *Biochemistry 28*, 2134−2139.
49. Cooper, T. M., and Woody, R. W. (1990) *Biopolymers 30*, 657−676.
50. Su, J. Y., Hodges, R. S., and Kay, C. M. (1994) *Biochemistry 33*, 15501−15510.
51. Krimm, S., and Bandekar, J. (1986) *Adv. Protein Chem. 38*, 181−365.
52. Mendelsohn, R., and Mantsch, H. H. (1986) in *Progress in Lipid-Protein Interactions* (Watts, A., and DePont, J. J. H. H. M., Eds.) Vol. 1, pp 103−146, Elsevier, Amsterdam.
53. Arrondo, J. L. R., Muga, A., Castresana, J., and Goñi, F. M. (1993) *Prog. Biophys. Mol. Biol. 59*, 23−56.
54. Chirgadze, Yu. N., Fedorov, O. V., and Trushina, N. P. (1975) *Biopolymers 14*, 679−694.
55. Venyaminov, S. Yu., and Kalnin, N. N. (1990) *Biopolymers 30*, 1243−1257.
56. Venyaminov, S. Yu., and Kalnin, N. N. (1990) *Biopolymers 30*, 1259−1271.
57. Rothschild, K. J., and Clark, N. A. (1979) *Science 204*, 311−312.
58. Dwivedi, A. M., and Krimm, S. (1984) *Biopolymers 2*, 923−943.
59. Tatulian, S. A., Biltonen, R. L., and Tamm, L. K. (1997) *J. Mol. Biol. 268*, 809−815.
60. Barnett, S. M., Edwards, C. M., Butler, I. S., and Levin, I. W. (1997) *J. Phys. Chem. B 101*, 9421−9424.
61. Voss, J. C., Jones, L. R., and Thomas, D. D. (1994) *Biophys. J. 67*, 190−196.
62. Ferrington, D. A., Yao, Q., Gilger, P. L., and Bigelow D. J. (2002) *J. Biol. Chem.* (submitted for publication).
63. Yao, Q., Chen, L. T., Li, J., Brundardt, K., Squier, T. C., and Bigelow, D. J. (2001) *Biochemistry 40* (in press).
64. Simmerman, H. K. B., Lovelace, D. E., and Jones, L. R. (1989) *Biochim. Biophys. Acta 997*, 322−329.
65. Villalaín, J., Gómez-Fernández, J. C., Jackson, M., and Chapman, D. (1989) *Biochim. Biophys. Acta 978*, 305−312.
66. Arkin, I. T., Rothman, M., Ludlam, C. F. C., Aimoto, S., Engelman, D. M., Rothschild, K. J., and Smith, S. O. (1995) *J. Mol. Biol. 248*, 824−834.
67. Echabe, I., Dornberger, U., Prado, A., Goñi, F. M., and Arrondo, J. L. (1998) *Protein Sci. 7*, 1172−1179.
68. Vorherr, T., Wrzosek, A., Chiesi, M., and Carafoli, E. (1993) *Protein Sci. 2*, 339−347.
69. Lamberth, S., Schmid, H., Muenchbach, M., Vorherr, T., Krebs, J., Carafoli, E., and Griesinger, C. (2000) *Helv. Chim. Acta 83*, 2141−2152.
70. Williams, R. W., McIntyre, J. O., Gaber, B. P., and Fleischer, S. (1986) *J. Biol. Chem. 261*, 14520−14524.
71. Hunter, G. W., Bigelow, D. J., and Squier, T. C. (1999) *Biochemistry 38*, 4604−4612.
72. Negash, S., Huang, S., and Squier, T. C. (1999) *Biochemistry 38*, 8150−8158.
73. Huang, S., and Squier, T. C. (1998) *Biochemistry 37*, 18064−18073.
74. Kimura, Y., Asahi, M., Kurzydlowski, K., Tada, M., and MacLennan, D. H. (1998) *J. Biol. Chem. 273*, 14238−14241.
75. Cornea, R. L., Jones, L. R., Autry, J. M., and Thomas, D. D. (1997) *Biochemistry 36*, 2960−2967.
76. Li, H., Cocco, M. J., Steitz, T. A., and Engelman, D. M. (2001) *Biochemistry 40* (in press).

BI011148D